Coexistence of Fermi Arcs and Fermi Pockets in High Temperature Cuprate Superconductors

Jianqiao Meng[1], Guodong Liu[1], Wentao Zhang[1], Lin Zhao[1], Haiyun Liu[1], Xiaowen Jia[1], Daixiang Mu[1], Shanyu Liu[1], Xiaoli Dong[1], Jun Zhang[1], Wei Lu[1], Guiling Wang[2], Yong Zhou[2], Yong Zhu[2], Xiaoyang Wang[2], Zuyan Xu[2], Chuangtian Chen[2] and X. J. Zhou[1,*]

[1]*National Laboratory for Superconductivity, Beijing National Laboratory for Condensed Matter Physics, Institute of Physics, Chinese Academy of Sciences, Beijing 100190, China*

[2]*Technical Institute of Physics and Chemistry, Chinese Academy of Sciences, Beijing 100190, China*

(Dated: May 14, 2009)

In the pseudogap state of the high$-T_c$ copper-oxide (cuprate) superconductors[1], angle-resolved photoemission (ARPES) measurements have seen an Fermi arc, i.e., an open-ended gapless section in the large Fermi surface[2, 3, 4, 5, 6, 7, 8], rather than a closed loop expected of an ordinary metal. This is all the more puzzling because Fermi pockets (small closed Fermi surface features) have been suggested from recent quantum oscillation measurements[9, 10, 11, 12, 13, 14]. The Fermi arcs have worried the high$-T_c$ community for many years because they cannot be understood in terms of existing theories. Theorists came up with a way out in the form of conventional Fermi surface pockets associated with competing order, with a back side that is for detailed reasons invisible by photoemission[15]. Here we report ARPES measurements of La-Bi2201 that give direct evidence of the Fermi pocket. The charge carriers in the pocket are holes and the pockets show an unusual dependence upon doping, namely, they exist in underdoped but not overdoped samples. A big surprise is that these Fermi pockets appear to coexist with the Fermi arcs. This coexistence has not been expected theoretically and the understanding of the mysterious pseudogap state in the high-T_c cuprate superconductors will rely critically on understanding such a new finding.

The high resolution Fermi surface mapping (Fig. 1a) on the underdoped La-Bi2201 UD18K sample using VUV laser reveals three Fermi surface sheets with low spectral weight (labeled as LP, LS and LPS in Fig. 1a) in the covered momentum space, in addition to the prominent main Fermi surface (LM). One particular Fermi surface sheet LP crosses the main band LM, forming an enclosed loop, an Fermi pocket, near the nodal region. Quantitative Fermi surface data measured from both VUV laser (Fig. 2a) and Helium discharge lamp (Fig. 2b) are summarized in Fig. 2c. All the possible umklapp bands[17], shadow bands[18], and umklapp bands of the shadow bands that may be present in the bismuth-based compounds, are shown for comparison (see Supplementary and SFig. 2 for more details). It is clear that the LP and LPS bands observed in VUV laser measurement (Fig. 2a) and HP band observed in Helium lamp measurement (Fig. 2b) are intrinsic; they can not be attributed to any of the umklapp bands or shadow bands (Fig. 2c). The location of the three bands can be well connected by the same superlattice vector, indicating that the HP and LPS bands correspond to the first order umklapp bands of the main Fermi pocket LP. The shape

and area of the Fermi pockets are also consistent in these two independent measurements, making a convincing case on the presence of the Fermi pocket. We note that in both the laser (Fig. 2a) and Helium lamp (Fig. 2b and SFig. 2 in the Supplementary) measurements, all the observed bands except for the "Fermi pocket bands" can be assigned by only one regular superstructure wavevector (0.24,0.24). The presence of additional superstructure, which would give rise to new bands, appears to be unlikely because there is no indication of such additional bands observed in our measurements.

The Fermi pocket is observed both in the normal state and superconducting state, as shown in Fig. 3 for the La-Bi2201 UD18K sample. Moreover, its location, shape and area show little change with temperature (Figs. 3a and 3f). Below T_c, the opening of superconducting gap is clearly observed on both the main band (Fig. 3c) and the back-side of the Fermi pocket (Fig. 3e). Above T_c, a portion of the main Fermi surface near the nodal region becomes gapless as indicated by the pink solid circles on the main Fermi surface (Fig. 3f). This is reminiscent to the Fermi arc (an open-ended gapless section in the large Fermi surface) formation in previous ARPES results which show an increase in the arc length with increasing temperature[3, 5]. The back side of the Fermi pocket also becomes gapless above T_c (Fig. 3j), forming a gapless Fermi pocket loop with part of the main band. We note that the Fermi arc on the main band appears to extend longer than the Fermi pocket section (Fig. 3f), giving rise to an interesting coexistence of Fermi arc and Fermi pocket.

The Fermi pocket exhibits an unusual doping dependence, as seen in Fig. 4. It is observed not only in the UD18K sample (Fig. 4b), but also in the UD26K sample (Fig. 4c). But it is not seen in the UD3K sample (Fig. 4a) and OP32K optimally-doped sample (Fig. 4d)[20]. This peculiar doping dependence of the Fermi pocket, i.e., it can only be observed in a limited doping range in the underdoped region, lends further support to its intrinsic nature. The quantitative main Fermi surface and Fermi pocket at various dopings are summarized in Fig. 4i. The area enclosed by the Fermi pockets in the UD18K (blue ellipse in Fig. 4i) and UD26K (grey ellipse in Fig. 4i) samples corresponds to a doping level of 0.11 and 0.12 holes/site, respectively, which is in good agreement with the estimated hole concentration of each sample[21, 22].

The Fermi pocket we have observed is hole-like. This makes it impossible to correspond to the electron-like Fermi pocket suggested from quantum oscillation experiments[11, 24]. Moreover, the observed Fermi pocket is not symmetrically located in the Brillouin zone,

specifically, it is not centered around ($\pi/2$,$\pi/2$) (Fig. 4i). This is distinct from that reported in Nd$-$LSCO system[23] which is symmetrical with respect to the (π,0)$-$(0,π) line, similar to the "shadow band" commonly observed in Bi2201 and Bi2212[18]. This particular location makes it impossible to originate from the *d*-density-wave "hidden order" that gives a hole-like Fermi pocket centered around ($\pi/2$,$\pi/2$) point[24, 25]. Among other possible origins of Fermi pocket formation[26, 27, 28], the phenomenological resonant valence bond picture[27] shows a fairly good agreement with our observations, in terms of the location, shape and area of the hole-like Fermi pocket and its doping dependence. In particular, the predicted Fermi pockets are pinned at ($\pi/2$,$\pi/2$) point[27] that is consistent with our experiment (Fig. 4i). One obvious discrepancy is that the spectral weight on the back side of the Fermi pocket near ($\pi/2$,$\pi/2$) is expected to be zero from these theories[26, 27] which is at odds with our measurements (Figs. 3d and 3i). We note that the existence of incommensurate density wave could also potentially explain the observed pockets. One possible wave-vector needed is (1 ± 0.092,1 ± 0.092) which is diagonal that can be examined by neutron or X-ray scattering measurements. There are indications of the charge-density-wave (CDW) formation reported in the Bi2201 system[29]; whether the Fermi surface reconstruction caused by such a CDW order or its related spin-density-wave order can account for our observation needs to be further explored.

One peculiar characteristic of the Fermi pocket is its coexistence with the large underlying Fermi surface (Figs. 3 and 4). One may wonder whether this could originate from sample inhomogeneity, i.e, the large Fermi surface is caused by a phase at high doping while the Fermi pocket is from a phase at low doping. We believe this is unlikely because there is no indication of two distinct superconducting phases detected in the magnetization measurement (SFig. 1 in the Supplementary). In addition, no Fermi pocket is identified for the underdoped UD3K sample (Fig. 4a). A more surprising observation is the coexistence of Fermi arcs and Fermi pockets in the normal state because it has not been expected theoretically. These new findings will provide key insight for understanding the anomalous pseudogap state in high-T_c cuprate superconductors.

---

[1] Timusk T. & Statt B. The pseudogap in high-temperature superconductors: an experimental survey. Rep. Prog. Phys. **62**, 61-122 (1999).

[2] Marshall, D. S. et al. Unconventional electronic structure evolution with hole doping in $Bi_2Sr_2CaCu_2O_{8+\delta}$: angle-resolved photoemission results. Phys. Rev. Lett. **76**, 4841-4844 (1996).

[3] Norman, M. R. et al. Destruction of the Fermi surface in underdoped high-Tc superconductors. Nature (London) **392**, 157-160 (1998).

[4] Shen, K. M. et al. Nodal quasiparticles and antinodal charge ordering in $Ca_{2-x}Na_xCuO_2Cl_2$. Science **307**, 901-904 (2005).

[5] Kanigel, A. et al. Evolution of the pseudogap from Fermi arcs to the nodal liquid. Nature Phys. **2**, 447-451 (2006).

[6] Lee, W. S. et al. Abrupt onset of a second energy gap at the superconducting transition of underdoped Bi2212. Nature (London) **450**, 81-84 (2007).

[7] Hossain, M. A. et al. *In situ* doping control of the surface of high-temperature superconductors. Nature Phys. **4**, 527-531 (2008).

[8] Yang, H. B. et al. Emergence of preformed Cooper pairs from the doped Mott insulating state in $Bi_2Sr_2CaCu_2O_{8+\delta}$. Nature (London) **456**, 77-80 (2008).

[9] Doiron-Leyraud, N. et al. Quantum oscillations and the Fermi surface in an underdoped high-Tc superconductor. Nature (London) **447**, 565-568 (2007).

[10] Bangura, A. et al. Small Fermi surface pockets in underdoped high temperature superconductors: Observation of ShubnikovCde Haas oscillations in $YBa_2Cu_4O_8$. Phys. Rev. Lett. **100**, 047004/1-4 (2008).

[11] LeBoeuf, D. et al. Electron pockets in the Fermi surface of hole-doped high-T_c superconductors. Nature (London) **450**, 533-536 (2007).

[12] Yelland, E. A. et al. Quantum oscillations in the underdoped cuprate $YBa_2Cu_4O_8$. Phys. Rev. Lett. **100**, 047003/1-4 (2008).

[13] Jaudet, C. et al. de Haas−van Alphen oscillations in the underdoped high temperature $YBa_2Cu_3O_{6.5}$. Phys. Rev. Lett. **100**, 187005/1-4 (2008).

[14] Sebastian, S. E. et al. A multi-component Fermi surface in the vortex state of an underdoped high-Tc superconductor. Nature (London) **454**, 200-203 (2008).

[15] Chakravarty, S., Nayak, C. & Tewari, S. Angle-resolved photoemission spectra in the cuprates from the d-density wave theory. Phys. Rev. B **68**, 100504/1-4 (2003).

[16] Ding, H. et al. Evolution of the Fermi surface with carrier concentration in $Bi_2Sr_2CaCu_2O_{8+\delta}$.

Phys. Rev. Lett. **78**, 2628-2631 (1997).

[17] Ding, H. et al. Momentum dependence of the superconducting gap in $Bi_2Sr_2CaCu_2O_8$. Phys. Rev. Lett. **74**, 2784 (1995); Osterwalder, J. et al. Angle-resolved photoemission experiments on $Bi_2Sr_2CaCu_20_{8+\delta}$ (001): Effects of the incommensurate lattice modulation. Appl. Phys. A **60**, 247-254 (1995).

[18] Aebi, P. et al. Complete Fermi surface mapping of $Bi_2Sr_2CaCu_2O_{8+x}$(001): Coexistence of short range antiferromagnetic correlations and metallicity in the same phase. Phys. Rev. Lett. **72**, 2757-2760 (1994); Nakayama, K. et al. Shadow bands in single-layered $Bi_2Sr_2CuO_{6+\delta}$ studied by angle-resolved photoemission spectroscopy. Phys. Rev. B **74**, 054505/1-6 (2006).

[19] Norman, M. R., Randeria, M., Ding H. & Campuzano, J. C. Phenomenology of the low-energy spectral function in high-T_c superconductors. Phys. Rev. B **57**, R11093-R11096 (1998).

[20] Meng, J. Q. et al. Monotonic d-wave superconducting gap of the optimally doped $Bi_2Sr_{1.6}La_{0.4}CuO_6$ superconductor by laser-based angle-resolved photoemission spectroscopy. Phys. Rev. B **79**, 024514/1-4 (2009).

[21] Meng, J. Q. et al. Growth, characterization and physical properties of high-quality large single crystals of $Bi_2(Sr_{2-x}La_x)CuO_{6+\delta}$ high-temperature superconductors. Supercond. Sci. Technol. **22**, 045010/1-6 (2009).

[22] Ono S. & Ando, Y. Evolution of the resistivity anisotropy in $Bi_2Sr_{2-x}La_xCuO_{6+\delta}$ single crystals for a wide range of hole doping. Phys. Rev. B **67**, 104512/1-9 (2003).

[23] Chang, J. et al. Electronic structure near the 1/8−anomaly in La−based cuprates. New Journ. Phys. **10**,103016/1-14 (2008).

[24] Chakravarty, S. & Kee, H. Y. Fermi pockets and quantum oscillations of the Hall coefficient in high-temperature superconductors. Proc. Natl. Acad. Sci. USA **105**, 8835-8839 (2008).

[25] Chakravarty, S., Laughlin, R. B., Morr, D. K. & Nayak, C. Hidden order in the cuprates. Phys. Rev. B **63**, 094503/1-10 (2001).

[26] Wen, X. G. & Lee, P. A. Theory of underdoped cuprates. Phys. Rev. Lett. **76**, 503-506 (1996).

[27] Yang, K. Y., Rice, T. M. & Zhang, F. C. Phenomenological theory of the pseudogap state. Phys. Rev. B. **73**, 174501/1-10 (2006); Ng, T.-K. Spinon-holon binding in t-J model. Phys. Rev. B **71**, 172509/1-4 (2005).

[28] Kaul, R. K., Kim, Y. B., Sachdev S. & Senthil, T. Algebraic charge liquids. Nature Phys. **4**, 28-31 (2008).

[29] Wise, W. D. et al. Charge-density-wave origin of cuprate checkerboard visualized by scanning tunnelling microscopy. Nature Phys. **4**, 696-699 (2008).

Supplementary Information is linked to the online version of the paper at www.nature.com/nature.

Acknowledgements We thank D.-H. Lee, P. A. Lee, S. Sachdev, Z.-X. Shen, X. G. Wen, Z. Y. Weng, T. Xiang, G. M. Zhang and F. C. Zhang for helpful discussions. This work is supported by the NSFC, the MOST of China, and Chinese Academy of Sciences.

Author Contributions J.Q.M. contributed to La-Bi2201 sample growth with the assistance of G.D.L.. X.L.D. and W.L. contributed to the magnetic measurement of samples. G.D.L, W.T.Z, L.Z., H.Y.L., J.Q.M., X.L.D., X.W.J., D.X.M., S.Y.L, J.Z., G.L.W., Y.Zhou, Y.Zhu, X.Y.W., Z.Y.X. and C.T.C contributed to the development and maintenance of Laser-ARPES system. J.Q.M. carried out the experiment with the assistance from G.D.L., W.T.Z., L.Z., H.Y.L., X.W.J., D.X.M., S.Y.L.. X.J.Z. and J.Q.M. analysed the data and wrote the paper. X.J.Z. are responsible for overall project direction, planning, management and infrastructure.

Author Information Reprints and permissions information is available at www.nature.com/reprints. Correspondence and requests for materials should be addressed to X.J.Z. (XJZhou@aphy.iphy.ac.cn).

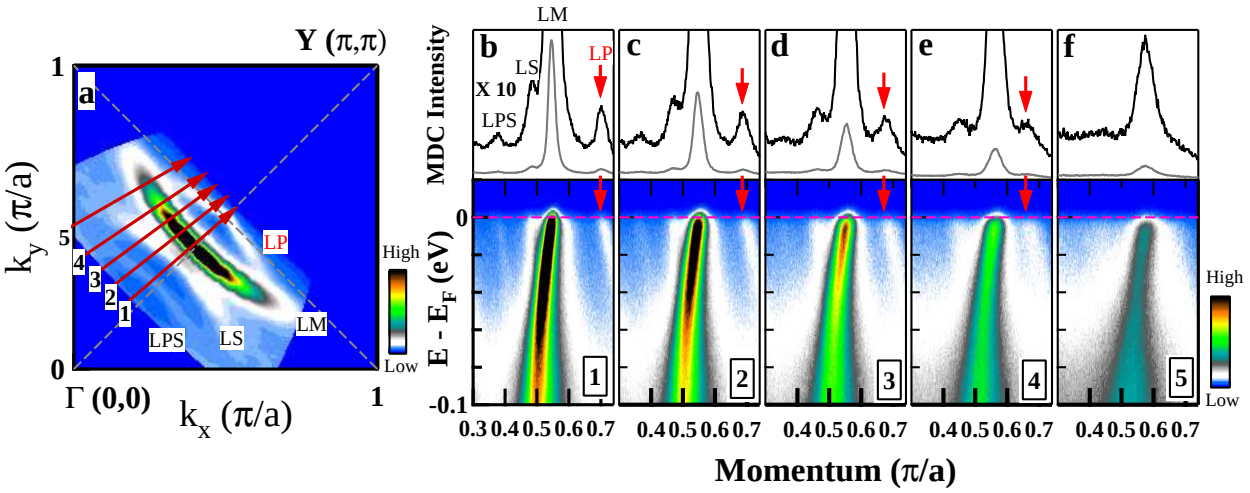

FIG. 1: Fermi surface and band structure of a La-Bi2201 sample. In the present paper, we use the phrase "Fermi surface" loosely to denote the momentum space locus of high intensity low-energy spectral weight. In cuprate superconductors, the Fermi surface is usually measured in the superconducting state in spite of the gap opening because the sharpness of the features at low temperature facilitates the precise determination of the underlying Fermi surface as compared to the normal state. It has been shown that the "underlying Fermi surface" determined from the minimum gap locus in the superconducting state is identical to that in the normal state[16]. (a). Photoemission intensity at the Fermi energy (E_F) as a function of k_x and k_y for the La-Bi2201 UD18K sample (underdoped, T_c=18 K) measured at a temperature of 14 K. It is obtained by symmetrizing the original data with respect to the (0,0)-(π,π) line. Four Fermi surface sheets are resolved in the covered momentum space, marked as LM for the main sheet, LP for the Fermi pocket, and LS and LPS for the others. (b-f) show band structure (bottom panels) and corresponding momentum distribution curves (MDCs) at the Fermi level (upper panels) along five typical momentum cuts (cuts 1 to 5) as labeled in Fig. 1a. To see the weak features more clearly, the original MDCs (thin grey lines) in the upper panel are expanded 10 times and plotted in the same figures (thick black lines). Note that the signal of the Fermi pocket LP is very weak; its intensity is over one order of magnitude weaker than that of the main band LM.

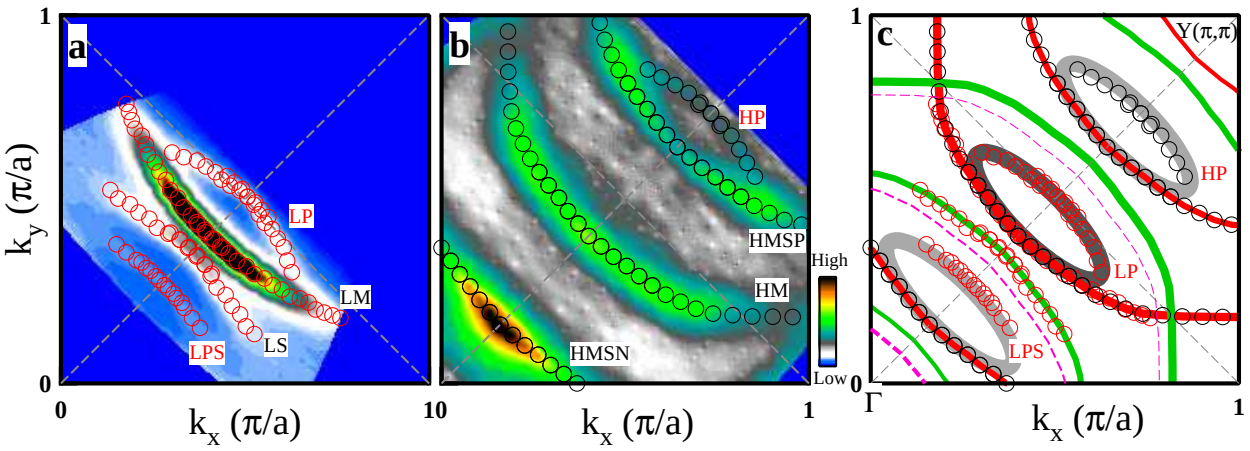

FIG. 2: Identification of the Fermi pocket in the photoemission data. (a). Fermi surface measured in the La-Bi2201 UD18K sample by the VUV laser. The four observed Fermi surface sheets in the covered momentum space are quantitatively represented by red circles. (b). Fermi surface measured in the La-Bi2201 UD18K sample by Helium discharge lamp at a photon energy of 21.218 eV. It is obtained by symmetrizing the original data with respect to the (0,0)-(π,π) line. Black circles represent quantitative positions of the observed Fermi surface sheets. (c). Summary of the measured Fermi surface from VUV laser (red empty circles, as in Fig. 2a) and Helium discharge lamp (black empty circles, as in Fig. 2b). Red lines represent the main Fermi surface (central thickest line) and its corresponding umklapp bands (thinner lines on either side of the main Fermi surface). The thickest green line represents the shadow band of the main Fermi surface, and thinner green lines the umklapp bands of the shadow band. The pink dashed lines represent possible high order umklapp bands from the main band in the third quadrant (see Supplementary and SFig. 2 for more details). It is clear that the main Fermi surface measured from the VUV laser (LM) shows a good agreement with that from the Helium discharge lamp (HM). The LS band observed in VUV laser agrees well with the first order umklapp band of the shadow band. The HMSP and HMSN bands observed in Helium discharge lamp measurements obviously correspond to the first order umklapp bands of the main band. The three ellipses represent the position of the observed Fermi pockets. The matrix element effect associated with photoemission process on the relative spectral intensity between the main band and Fermi pocket is an interesting issue to be further explored.

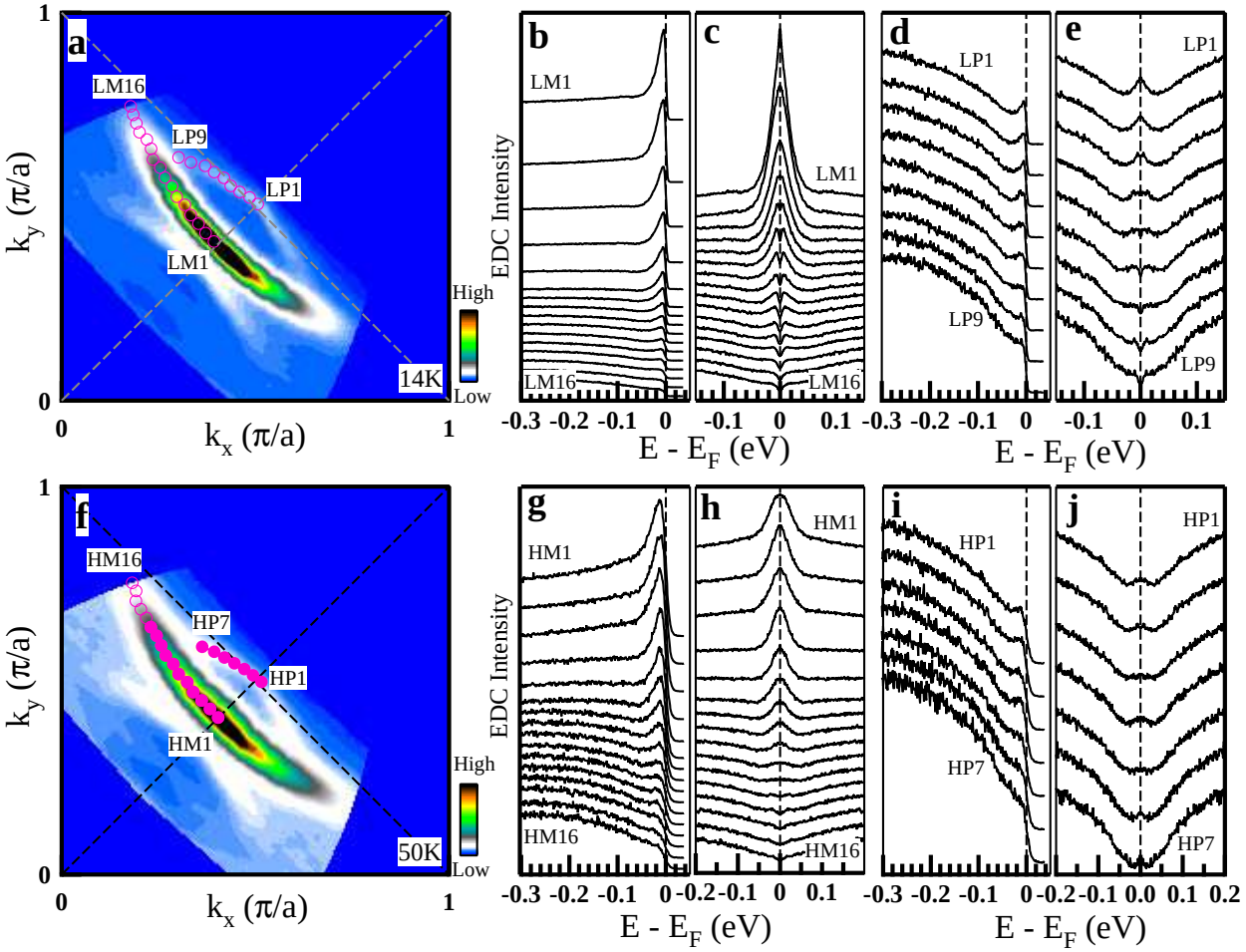

FIG. 3: Temperature dependence of the Fermi pocket. The top (bottom) panels show Fermi surface and photoemission spectra for the La-Bi2201 UD18K sample below T_c (above T_c). (a). Fermi surface mapping at 14 K. (b). Photoemission spectra (Energy Distribution Curves, EDCs) along the main Fermi surface. Sharp peaks are observed near the nodal region while they get weaker when moving to the antinodal region. (c). The corresponding symmetrized EDCs. The symmetrization procedure[19] provides an intuitive way in identifying an energy gap opening which is characterized by the appearance of a dip near the Fermi level while zero gap corresponds to a peak at the Fermi level. The gap size is determined by the EDC peak position with respect to the Fermi level. It is clear to see the gap opening and gap increase from the nodal to antinodal regions. (d). EDCs along the back side of the Fermi pocket. (e). The corresponding symmetrized EDCs. The gap opening and gap increase are also clear from the nodal to antinodal regions along the pocket. (f). Fermi surface mapping at 50 K. (g). EDCs along the main Fermi surface. (h). The corresponding symmetrized EDCs. At 50 K, there is a gapless region formed near the nodal region with its location denoted in (f) by pink solid circles while the main Fermi surface beyond this region remains gapped. (i). EDCs along the Fermi pocket. (j). The corresponding symmetrized

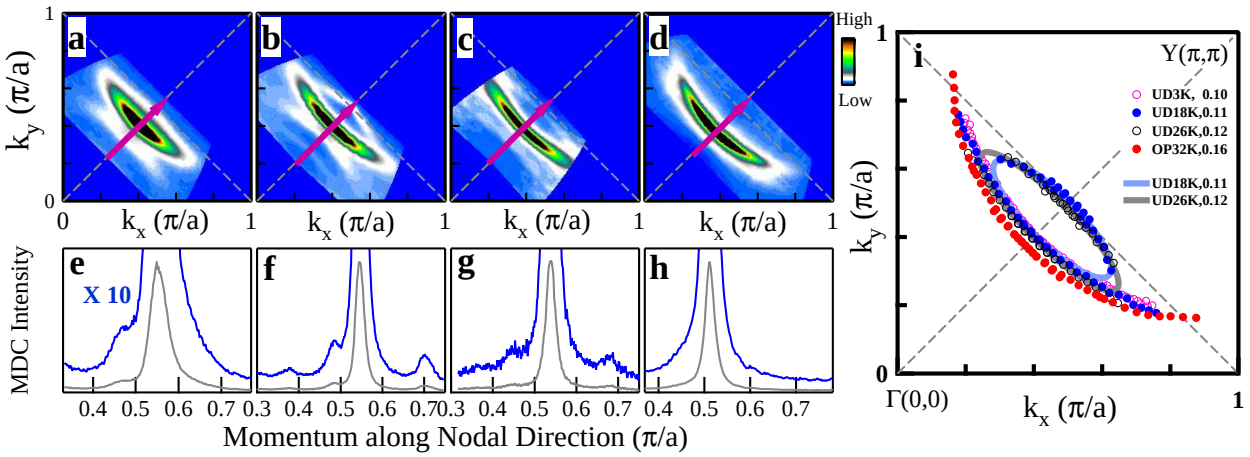

FIG. 4: Doping evolution of Fermi surface topology in La-Bi2201. (a-d) show Fermi surface mapping of UD3K (underdoped, T_c∼3 K), UD18K, UD26K (underdoped, T_c=26 K) and OP32K (optimally-doped, T_c=32 K)[20] samples, respectively. They are obtained by symmetrizing the original data with respect to the (0,0)-(π,π) line. (e-h) show the corresponding MDCs at the Fermi energy along the (0,0)-(π,π) nodal direction. The location of the momentum cuts is labeled in (a-d) by purple lines with arrows. To show the weak features more clearly, the original MDCs (thin grey lines in bottom panels in e-h) are expanded by ten times and plotted in the same figures (blue thick lines). Note that we can not completely exclude the possibility on the presence of Fermi pocket in the UD3K sample (Fig. 4a). It is noted that the MDC width of the sample (Fig. 4e) is much wider than that of other dopings (Figs. 4f-h), leaving a possibility that weak signal of a Fermi pocket may get buried in the broad feature. (i) Quantitative Fermi surface of La-Bi2201 at various doping levels. The two "Fermi pockets" for UD18K and UD26K samples are obtained by fitting both sides of the data points with ellipses.